Robotica (2013) volume 31, pp. 875–886. © Cambridge University Press 2013
doi:10.1017/S0263574713000088

Parametrically excited inverted double pendulum and efficient bipedal walking with an upper body

Toyoyuki Honjo†*, Akinori Nagano‡ and Zhi-Wei Luo‡

†*Department of Computer Science and Systems Engineering, Graduate School of Engineering, Kobe University, 1-1 Rokkodai-cho, Nada, Kobe, Hyogo, 657-8501, Japan*
‡*Department of Computational Science, Graduate School of System Informatics, Kobe University, 1-1 Rokkodai-cho, Nada, Kobe, Hyogo, 657-8501, Japan*

(Accepted January 9, 2013. First published online: February 22, 2013)

SUMMARY
Walking locomotion involves complex movement of total center of mass. Not only the lower body behavior but also the upper body behavior affects the walking characteristics. Therefore, in this paper we derive the principle of parametrically excited inverted double pendulum to consider both lower body and upper body dynamics. We propose one approach to utilize the upper body behavior of the robot for energy efficient bipedal locomotion. In addition, we analyze the property of parametrically excited inverted double pendulum.

KEYWORDS: Dynamical bipedal walking; Parametrically excited inverted pendulum; Upper body control.

1. Introduction

In the field of robotic bipedal walking, one of the challenging tasks is to achieve energy efficient walking. It is important that the robot utilizes its dynamics and the external force from the environment for energy efficiency. As one of the most energy efficient walking approaches, passive dynamic walking has been proposed by McGeer.[1] In passive dynamic walking, a biped robot continuously and stably walks down a gentle slope without any actuators or mechanical inputs when the robot is placed on a suitable initial condition. The loss of mechanical energy is caused by the collision between the edge of the swing leg and the walking surface. In this walking approach, mechanical energy is restored by transporting potential energy to kinetic energy while descending the slope. However, bipedal walking on the level floor has no propulsion generated by gravity and cannot convert potential energy into kinetic energy. Therefore, mechanical energy must be restored through some mechanical inputs to realize bipedal walking on the level floor. Many control strategies to restore the mechanical energy have been proposed. One of these approaches for restoring mechanical energy is parametric excitation. Asano *et al.*[2–4] applied a parametric excitation principle to a biped robot with telescopical actuator in its legs to change the center of mass position of the swing leg. Harata *et al.*[5–7] proposed to apply parametric excitation to a biped robot with knee joint and semicircular feet. We proposed to apply parametric excitation of an inverted pendulum to a biped robot to consider whole body dynamics of the robot.[8] We dealt with the robot's total center of mass as an inverted pendulum and controlled the trajectory of mass center to be closer to the optimal trajectory of a parametrically excited inverted pendulum. In addition, we proposed a new target trajectory to realize more energy efficient walking.[9] This target trajectory is represented by a product of two sigmoid functions and the horizontal center of mass position. Using this target trajectory enables the robot to actuate its knee joint at the desired position. Parametric excitation of an asymmetric system is also studied. Hayashi *et al.*[15–17] studied the effect of counterweights. In addition, walking approaches based on the asymmetric posture of the lower body are researched.[18–21]

We have considered only the lower body behavior. However, walking locomotion involves complex movement of the total center of mass. The upper body behavior also affects the walking characteristics. Therefore, we should consider both lower body and upper body dynamics to generate more energy efficient walking. In general, adding an upper body causes additional control task to stabilize the upper body behavior and this control task leads to reduced energy efficiency. To avoid this problem, Wisse *et al.*[10,11] developed the bisecting hip mechanism to mechanically maintain the upper body upright. The upper body is maintained in the middle angle of the stance leg and the swing leg by the gear box and chains. This approach does not require control inputs for stabilizing the upper body. Narukawa *et al.*[12,13] proposed walking approaches for the bipedal walker with a torso. They verified the effect of PD control, optimal control with/without hip springs for the torso and achieved stable and efficient walking. Flynn *et al.*[22,23] proposed the dynamical walking with a torso which utilized the unbalance feature for locomotive power based on the idea of self-propelling disc. In this paper, we derive the parametric excitation principle of an inverted double pendulum to consider both lower body and upper body dynamics. Consequently, it is found that maintaining the upper pendulum in a constant forward tilted posture contributes to the increase of mechanical energy. In addition, we analyze the relationship between parametrically excited inverted double pendulum and parametrically excited inverted pendulum. As a result, it is found that the advantage of parametrically excited inverted double pendulum is

* Corresponding author. E-mail: carcharo-mack@cs11.cs.kobe-u.ac.jp

https://doi.org/10.1017/S0263574713000088 Published online by Cambridge University Press

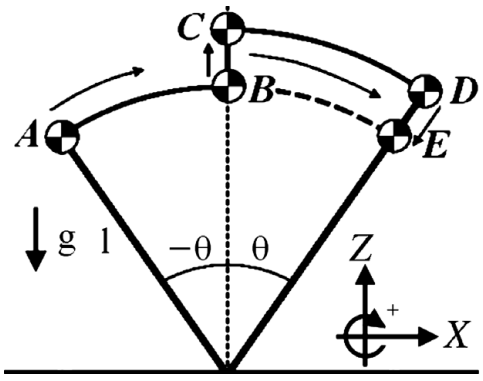


Fig. 1. The optimal trajectory of parametrically excited inverted pendulum.

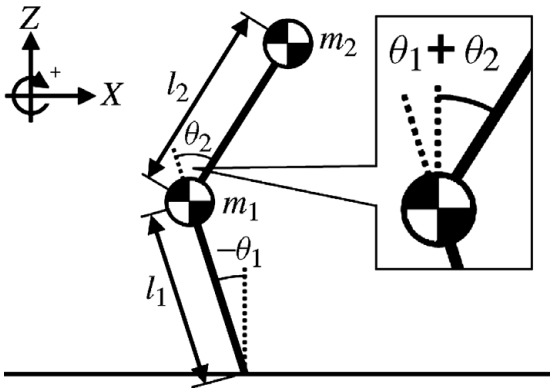


Fig. 2. The model of an inverted double pendulum.

equivalent to asymmetric property of parametrically excited inverted pendulum. Then we deal with the upper body and lower body of the robot as an inverted double pendulum. This virtual inverted double pendulum consists of the upper body mass and total center of mass of the lower body. We apply parametric excitation of an inverted double pendulum to this virtual inverted double pendulum. In this case the robot controls its upper body to keep the virtual upper pendulum constant. We verify the validity of the proposed parametric excitation for bipedal walking via numerical simulation. As a result, although the angle of the upper pendulum is maintained in a constant value, the upper body behavior has the characteristics similar to sine curves. In addition, when the desired angle of the upper pendulum enlarges, the robot achieves more energy efficient walking. We found that our method enables the robot to achieve the stable walking whose efficiency is close to human walking. In addition, the robot also achieves the stable walking whose efficiency is similar to or greater than other bipedal walkers with the upper body.[23−25] Therefore, we suggest that parametrically excited inverted double pendulum is valid for achieving energy efficient walking.

2. Parametric Excitation of an Inverted Double Pendulum

2.1. Parametric excitation of an inverted pendulum

The simple example of parametric excitation is a swing at a park. When we play on a swing, we bend and stretch our knee to increase the amplitude of the swing. In this situation, we control our center of mass position using our knee. In some walking approaches, parametric excitation principle has been applied to the swing leg of a biped robot.[2−7] The optimal trajectory of parametric excitation for a pendulum has been proposed by Lavrovskii *et al.*[14] However, when the robot achieves stable walking, not only the swing leg mass but also the total center of mass moves forward. Therefore, we dealt with the robot's total center of mass as a virtual inverted pendulum. Then we applied parametric excitation of an inverted pendulum to this virtually inverted pendulum.[8,9] We derived the optimal trajectory of parametrically excited inverted pendulum and this trajectory is shown in Fig. 1. Based on the assumption that the length of the inverted pendulum can be changed instantaneously, this trajectory is derived. The equation related to the kinetic energy of this inverted pendulum is described as

$$\begin{aligned} K &= \frac{1}{2}ml^2\dot{\theta}^2, \\ L &= ml^2\dot{\theta}, \\ \dot{L} &= mgl\sin\theta, \end{aligned} \tag{1}$$

where m is the mass of the inverted pendulum, l is the length of the inverted pendulum, θ is the angle of the inverted pendulum from the vertical axis, and g is the gravitational acceleration. K is the kinetic energy and L is the angular momentum. From Eq. (1), during $\theta < 0$, kinetic energy and angular momentum of the inverted pendulum is reduced because $\dot{L}$ becomes a negative value. During $\theta \geq 0$, kinetic energy and angular momentum of the inverted pendulum is increased because $\dot{L}$ becomes a positive value. The increase of mechanical energy $\Delta E := E^+ - E^-$ is derived as the difference between the amount of increased energy E^+ ($\theta \geq 0$) and the amount of decreased energy E^- ($\theta < 0$). Consequently, the length of the inverted pendulum is made longer to increase E^+ during $\theta \geq 0$.

2.2. Parametric excitation of an inverted double pendulum

We introduce parametric excitation of an inverted double pendulum. The model of an inverted double pendulum in this paper is shown in Fig. 2. This inverted double pendulum consists of two rigid bars (the lower and upper pendulum). l_1 and l_2 are the length of lower and upper pendulum respectively, and m_1 and m_2 are the mass of lower and upper pendulum respectively. θ_1 is the angle of the lower pendulum from the vertical axis. θ_2 is the relative angle of the upper pendulum from the lower pendulum. As shown in Fig. 2, $\theta_1 + \theta_2$ is the absolute angle of the upper pendulum from the vertical axis.

Kinetic energy K and angular momentum $\boldsymbol{L}$ of this inverted double pendulum are described as

$$\begin{aligned} K &= \frac{1}{2}\dot{\boldsymbol{q}}^{\mathrm{T}}\boldsymbol{M}(\boldsymbol{q})\dot{\boldsymbol{q}}, \\ \boldsymbol{L} &= \boldsymbol{M}(\boldsymbol{q})\dot{\boldsymbol{q}}, \\ \dot{\boldsymbol{L}} &= \dot{\boldsymbol{L}}_1 + \dot{\boldsymbol{L}}_2 + \dot{\boldsymbol{L}}_3, \end{aligned} \tag{2}$$

https://doi.org/10.1017/S0263574713000088 Published online by Cambridge University Press

where $\boldsymbol{q} = [\theta_1 \ \theta_2]^{\mathrm{T}}$ is the generalized coordinate vector. $\boldsymbol{M}(\boldsymbol{q})$ is the inertia matrix and described as

$$\boldsymbol{M}(\boldsymbol{q}) = \begin{bmatrix} m_1 l_1^2 + m_2\left(l_1^2 + l_2^2 + 2l_1 l_2 \cos\theta_2\right) & sym \\ m_2\left(l_2^2 + l_1 l_2 \cos\theta_2\right) & m_2 l_2^2 \end{bmatrix}. \tag{3}$$

In addition, $\dot{\boldsymbol{L}}_1$, $\dot{\boldsymbol{L}}_2$, and $\dot{\boldsymbol{L}}_3$ are described as

$$\begin{aligned} \dot{\boldsymbol{L}}_1 &= (m_1 + m_2)\, g l_1 \sin\theta_1 \begin{bmatrix} 1 \\ 0 \end{bmatrix}, \\ \dot{\boldsymbol{L}}_2 &= m_2 g l_2 \sin(\theta_1 + \theta_2) \begin{bmatrix} 1 \\ 1 \end{bmatrix}, \\ \dot{\boldsymbol{L}}_3 &= -m_2 l_1 l_2 \sin\theta_2 \dot{\theta}_1 \left(\dot{\theta}_1 + \dot{\theta}_2\right) \begin{bmatrix} 0 \\ 1 \end{bmatrix}. \end{aligned} \tag{4}$$

On the right side of $\dot{\boldsymbol{L}}$, the first term $\dot{\boldsymbol{L}}_1$ is the term of parametric excitation similar to the one that appeared in Eq. (1). Therefore, the lower pendulum is controlled based on parametric excitation of an inverted pendulum. When the upper pendulum is tilted forward ($\theta_1 + \theta_2 > 0$), the second term $\dot{\boldsymbol{L}}_2$ becomes a positive value and $\dot{\boldsymbol{L}}$ enlarges. Conversely, when the upper pendulum is tilted backward ($\theta_1 + \theta_2 < 0$), $\dot{\boldsymbol{L}}_2$ becomes a negative value and $\dot{\boldsymbol{L}}$ decreases. Therefore, maintaining the upper pendulum angle at a positive value ($\theta_1 + \theta_2 > 0$) contributes to parametric excitation. Lastly, the third term $\dot{\boldsymbol{L}}_3$ is affected by the angle and angular velocity of the inverted double pendulum. Therefore, it is difficult to explain the behavior of this term. However, when the angle of the upper pendulum does not change ($\dot{\theta}_1 + \dot{\theta}_2 = 0$), the third term $\dot{\boldsymbol{L}}_3$ becomes zero. From these analyses, we obtain the following two control strategies:

- The lower pendulum is controlled based on the parametric excitation of an inverted pendulum (the length of the lower pendulum l_1 is made longer during $\theta_1 \geq 0$).
- The upper pendulum is maintained in a positive constant angle ($\theta_1 + \theta_2 > 0$ and $\dot{\theta}_1 + \dot{\theta}_2 = 0$).

If these two conditions are satisfied, $\dot{\boldsymbol{L}}$ has only the parametrically excited term $\dot{\boldsymbol{L}}_1$ and the constant positive value of $\dot{\boldsymbol{L}}_2$.

2.3. Simulation of the inverted double pendulum

We control the inverted double pendulum based on the aforementioned two conditions. First, the desired length l_{1d} of the lower pendulum is given as

$$l_{1d}(x) = l_{1\star} + \frac{\hat{A}}{1 + e^{-\alpha(x-\beta_1)}} \times \frac{1}{1 + e^{\alpha(x-\beta_2)}}, \tag{5}$$

$$\dot{l}_{1d}(x) = \frac{\alpha \hat{A} \dot{x}\left(e^{-\alpha(x-\beta_1)} - e^{\alpha(x-\beta_2)}\right)}{\left[1 + e^{\alpha(\beta_1-\beta_2)} + e^{-\alpha(x-\beta_1)} + e^{\alpha(x-\beta_2)}\right]^2}, \tag{6}$$

$$\hat{A} = A\left(1 + 2e^{\alpha\frac{(\beta_1-\beta_2)}{2}} + e^{\alpha(\beta_1-\beta_2)}\right), \tag{7}$$

where $l_{1\star}$ is the initial length of the lower pendulum, A, α, β_1, and β_2 are parameters that determine the shape of the target function. A is the amplitude of this function, α is the parameter that determines the magnitude of lift and descent slope, and β_1 and β_2 are positions of lift and descent respectively. $\hat{A}$ is the normalization term of the amplitude A and x is the horizontal center of mass position of this system. This target function is represented by a product of two sigmoid functions.[9] Second, the target angle of the upper pendulum is given as

$$\begin{aligned} \theta_{2d} &= (\theta_{1\star} + \theta_{2\star}) - \theta_1, \\ \dot{\theta}_{2d} &= -\dot{\theta}_1, \end{aligned} \tag{8}$$

where $\theta_{i\star}$, $i = 1, 2$ are initial angles of the lower and upper pendulum respectively.

Table I. Physical parameters of the inverted double pendulum.

Name	Value (unit)	Name	Value (unit)
m_1	10.0 (kg)	m_2	1.00–5.00 (kg)
$l_{1\star}$	1.00 (m)	l_2	0.40–0.80 (m)
$\theta_{1\star}$	−0.40 (rad)	$\theta_{2\star}$	0.00–0.80 (rad)
A	0.05 (m)	α	50.0 (–)
β_1	−0.03 (m)	β_2	0.10 (m)

Table I shows physical parameters of the inverted double pendulum. We assume that the range of θ_1 is from −0.40 (rad) to 0.40 (rad).

Fig. 3 shows the simulation results. ΔE is the increased mechanical energy of the inverted double pendulum through the simulation. From Fig. 3, ΔE enlarged when the upper pendulum was maintained in a constant positive posture $\theta_1 + \theta_2 \geq 0$. Conversely, ΔE reduced when the upper pendulum was maintained in a constant negative posture $\theta_1 + \theta_2 < 0$. These results suit parametric excitation of an inverted double pendulum.

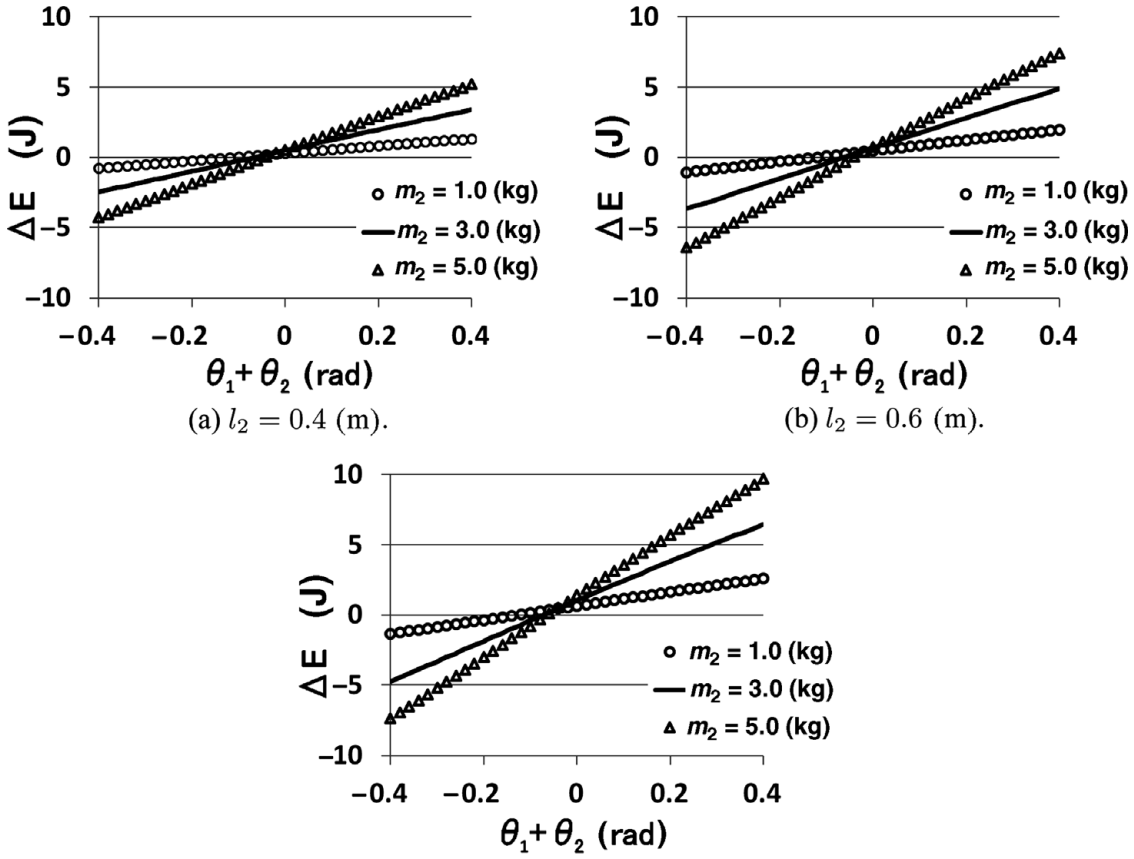
2.4. Asymmetric property of a virtual inverted pendulum

Recently, the walking performances with respect to the asymmetric posture of the lower body or the asymmetric inverted single pendulum with counterweights have been researched.[15–21] In this section, we analyzed the characteristics of parametric excitation of an inverted double pendulum. The inverted double pendulum is equivalent to a virtual inverted pendulum as shown in Fig. 4(a). The length l_{VP} and angle θ_{VP} of this virtual inverted pendulum are derived as

$$\begin{aligned} l_{\mathrm{VP}} &= \sqrt{l_1^2 + \left(\frac{m_2 l_2}{m_1 + m_2}\right)^2 + \frac{2m_2 l_1 l_2}{m_1 + m_2}\cos\theta_2}, \\ \theta_{\mathrm{VP}} &= \sin^{-1}\left(\frac{l_1 \sin\theta_1 + \frac{m_2 l_2}{m_1+m_2}\sin(\theta_1 + \theta_2)}{\sqrt{l_1^2 + \left(\frac{m_2 l_2}{m_1+m_2}\right)^2 + \frac{2m_2 l_1 l_2}{m_1+m_2}\cos\theta_2}}\right). \end{aligned} \tag{9}$$

From Eq. (9), phase difference $\Delta\theta_{\mathrm{VP}}$ between the initial angle θ_{VPI} and final angle θ_{VPF} of this virtual inverted pendulum

https://doi.org/10.1017/S0263574713000088 Published online by Cambridge University Press



(a) $l_2 = 0.4$ (m). (b) $l_2 = 0.6$ (m).

(c) $l_2 = 0.8$ (m).

Fig. 3. Increased mechanical energy ΔE with respect to three lengths l_2 and three point masses m_2 of the upper pendulum.

are derived as

$$\begin{aligned}\Delta\theta_{\mathrm{VP}} &= \theta_{\mathrm{VPF}} - (-\theta_{\mathrm{VPI}}) \\ &= \sin^{-1}\left(\frac{2m_2 l_2 Z_g}{(m_1+m_2) l_{\mathrm{VPF}} l_{\mathrm{VPI}}}\sin(\theta_1+\theta_2)\right), \end{aligned} \quad (10)$$

where l_{VPI} and l_{VPF} are the initial and final length of the virtual inverted pendulum, and Z_g is the initial vertical center of mass position of the virtual inverted pendulum.

From Eq. (10), the initial length and angle of this virtual inverted pendulum l_{VPI} and θ_{VPI} are equal to the final length and angle of this virtual pendulum l_{VPF} and θ_{VPF} if the upper pendulum is maintained in the vertical posture ($\theta_1 + \theta_2 = 0$) as shown in Fig. 4(b). In addition, this virtual inverted pendulum has asymmetric characteristics as shown in Figs. 4(c) and (d). Consequently, the interval of $\theta_{\mathrm{VP}} \geq 0$ becomes larger than the interval of $\theta_{\mathrm{VP}} < 0$ when the angle of the upper pendulum is maintained in a positive constant angle ($\theta_1 + \theta_2 > 0$, $\dot{\theta}_1 + \dot{\theta}_2 = 0$). In addition, the final length l_{VPF} becomes longer than the initial length l_{VPI} because the final height of mass center is the same as the initial height as shown in Fig. 5. From the principle of parametrically excited inverted pendulum, the larger interval of $\theta_{\mathrm{VP}} \geq 0$ and the longer length l_{VPF} increase the amount of ΔE. Therefore, the characteristic of parametrically excited inverted double pendulum is equivalent to asymmetric property of parametrically excited inverted pendulum.

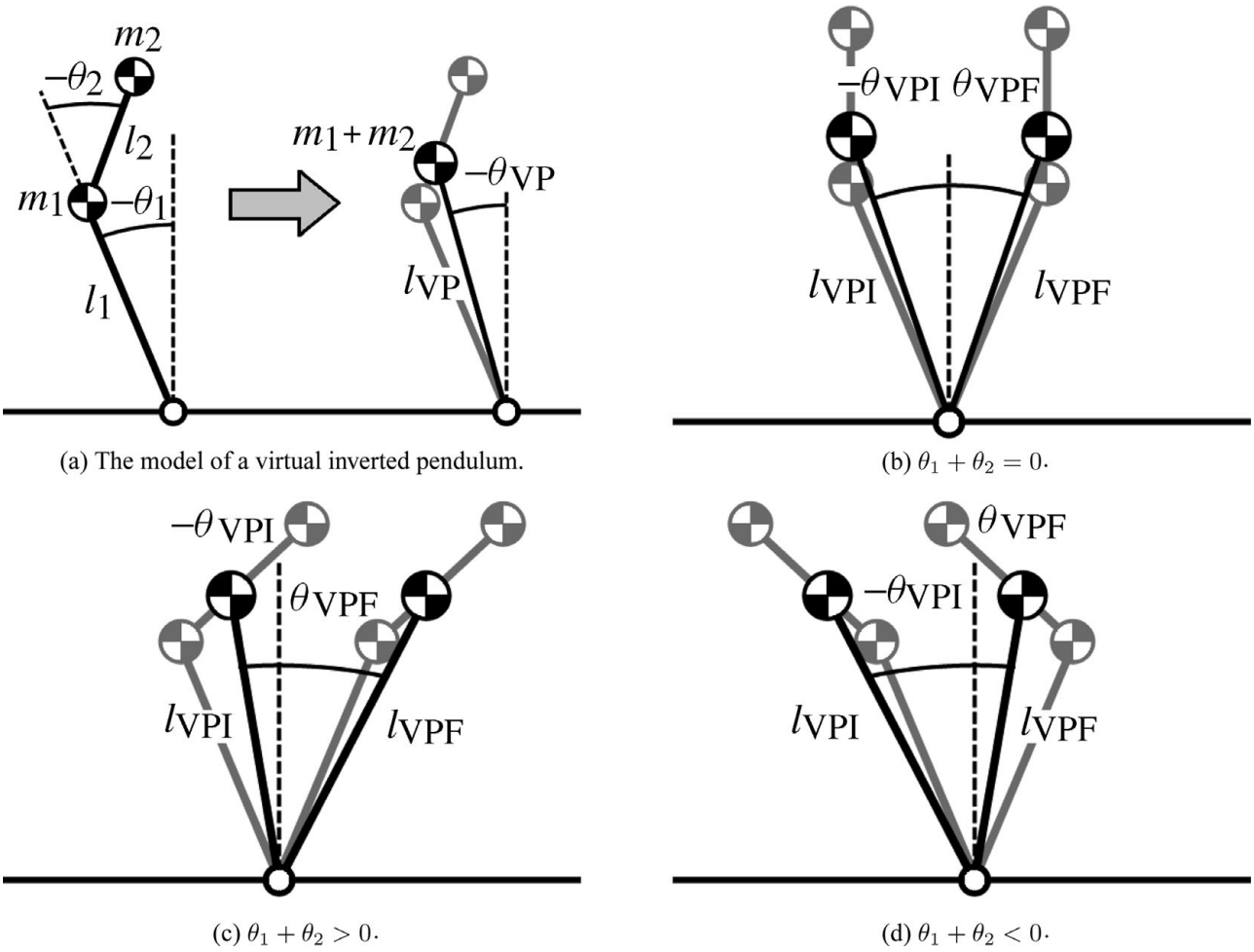
3. Simulation of Bipedal Walker with An Upper Body

In this section we describe the model of bipedal walker and control method to apply the control strategy of parametrically excited inverted double pendulum to the bipedal walker with a torso.

3.1. Model of bipedal walker with an upper body

Fig. 6 shows the model of planar bipedal walking robot in this paper. The leg of this robot consists of two rigid bars connected with each other by the knee joint. This leg has an arc-like foot whose center is located at the lower leg. In addition, the upper body of this robot is composed of one rigid bar whose mass is located on the edge. A pair of legs and the upper body are connected with each other by the hip joint. This robot has seven degrees of freedom (DOF): the position of the hip joint (x, z) and five angles of the upper body, and a pair of legs θ_i $(i = 0, \ldots, 4)$. The origin of world coordinate is located at the contact point between the vertical stance leg ($\theta_1 = \theta_2 = 0$(rad)) and the ground. We show the state transition diagram of dynamical walking in Fig. 7. As shown in this figure, dynamical walking of this robot has two phases and four states during one step. First, we explain the conditions of single support phase. During S1 and S3, the motion equation that represents the dynamics of this robot is calculated by numerical integration. The stance leg constantly contacts the walking surface and rotates around the contact point. The knee joint of the stance leg is locked in a straight posture by mechanical constraint. During S1,

https://doi.org/10.1017/S0263574713000088 Published online by Cambridge University Press



(a) The model of a virtual inverted pendulum.

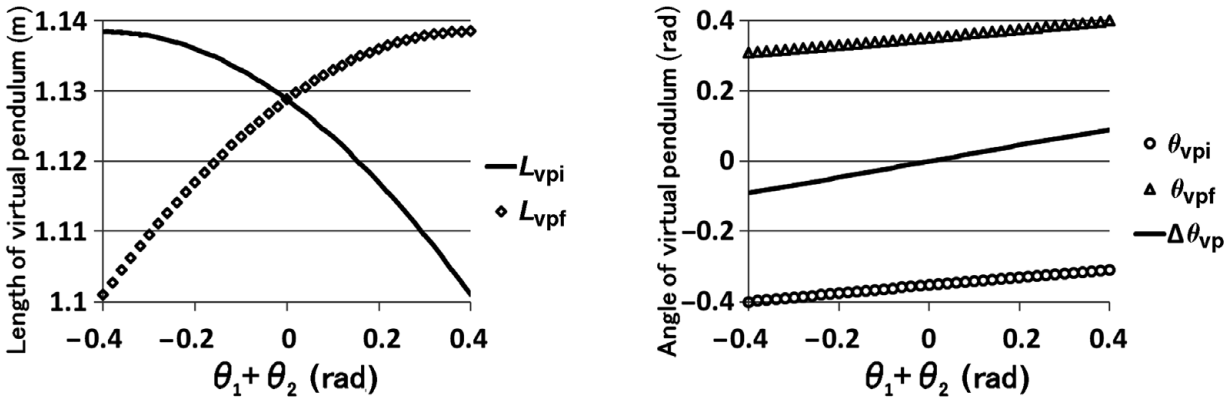
(b) $\theta_1 + \theta_2 = 0$.

(c) $\theta_1 + \theta_2 > 0$.

(d) $\theta_1 + \theta_2 < 0$.

Fig. 4. The relationship between initial state and final state of the virtual inverted pendulum. θ_{VP} and l_{VP} are the angle and length of a virtual inverted pendulum. Indexes VPI and VPF represent the initial and final states of a virtual inverted pendulum respectively.

the knee joint of the swing leg is free and the knee joint of the swing leg is bent and extended by control inputs. When the swing leg is fully extended, instantaneous knee collision occurs and S1 changes into S2. S2 is a discrete event and the effect of instantaneous impact is calculated by collision equation. In the instantaneous collision, the posture of this robot does not change. Only the velocity of this robot is updated. After updating the robot velocity, S2 changes into S3. During S3, the knee joint of the swing leg is locked in a straight posture. When the edge of the swing leg collides against the ground, the instantaneous ground collision occurs and S3 changes into S4. S4 is an instantaneous double support phase and the effect of instantaneous ground impact is calculated by collision equation. After double support



(a) Initial and final lengths of the virtual inverted pendulum L_{vpi} and L_{vpf}.

(b) Initial and final angles of the virtual inverted pendulum θ_{vpi} and θ_{vpf} and difference angle $\Delta\theta_{vp}$.

Fig. 5. The lengths and angles of the virtual inverted pendulum when $m_2 = 3.0$ (kg) and $l_2 = 0.6$ (m).

https://doi.org/10.1017/S0263574713000088 Published online by Cambridge University Press

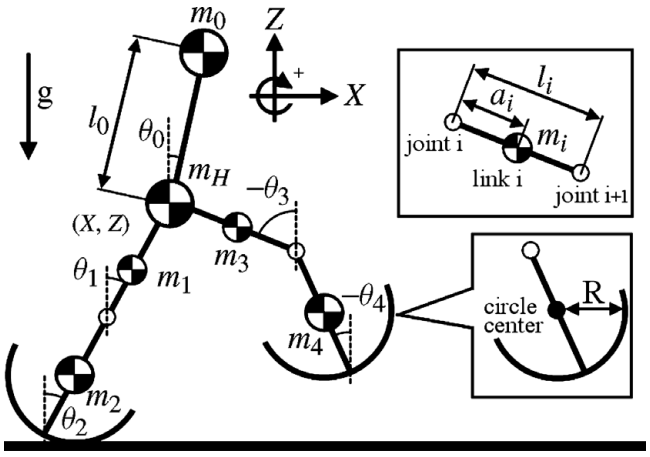


Fig. 6. The bipedal walking model with an upper body. a_i $(i = 1, \ldots, 4)$ is the length from joint i to the mass position of the link$_i$. l_i $(i = 1, \ldots, 4)$ is the length from joint i to joint $i + 1$.

phase, the stance leg changes into new swing leg and the swing leg changes into new stance leg. After updating robot velocity and exchanging the role of each leg, S4 changes into S1.

Motion equation of S1 and S3 is described as

$$\boldsymbol{M}(\boldsymbol{q})\ddot{\boldsymbol{q}} + \boldsymbol{h}(\boldsymbol{q}, \dot{\boldsymbol{q}}) = \boldsymbol{S}\boldsymbol{u} + \boldsymbol{J}_K^{\mathrm{T}}(\boldsymbol{q})\boldsymbol{\lambda}_K, \tag{11}$$

where $\boldsymbol{q} = [x, z, \theta_0, \theta_1, \theta_2, \theta_3, \theta_4]^{\mathrm{T}} \in \mathbb{R}^7$ is the generalized coordinate vector, $\boldsymbol{M} \in \mathbb{R}^{7\times7}$ is inertia matrix, $\boldsymbol{h} \in \mathbb{R}^7$ is the vector in which the Coriolis force, centrifugal force, and gravity term are included. $\boldsymbol{S}\boldsymbol{u} \in \mathbb{R}^7$ is control input to the knee joint of the swing leg and the upper body. $\boldsymbol{J}^{\mathrm{T}}(\boldsymbol{q})\boldsymbol{\lambda} \in \mathbb{R}^7$ is the constraint vector to keep the ground contact condition and make the leg straight. We assume that the edge of the stance leg does not slip or penetrate the walking surface. Therefore, these ground contact conditions are denoted as

$$\begin{aligned} x - l_1 \sin\theta_1 - (l_2 - R)\sin\theta_2 &= R\theta_2, \\ z - l_1 \cos\theta_1 - (l_2 - R)\cos\theta_2 - R &= 0. \end{aligned} \tag{12}$$

From Eq. (12), restraint conditions for the velocity are described as

$$\begin{aligned} \dot{x} - l_1 \cos\theta_1\dot{\theta}_1 - (l_2 - R)\cos\theta_2\dot{\theta}_2 - R\dot{\theta}_2 &= 0, \\ \dot{z} + l_1 \sin\theta_1\dot{\theta}_1 + (l_2 - R)\sin\theta_2\dot{\theta}_2 &= 0. \end{aligned} \tag{13}$$

In addition, the knee joint of the stance leg is locked in a straight posture by mechanical constraint. Constraint condition for the relative knee angle of the stance leg $\theta_{K1} = -(\theta_1 - \theta_2)$ is described as

$$-\left(\dot{\theta}_1 - \dot{\theta}_2\right) = 0. \tag{14}$$

Similarly, the knee joint of the swing leg is locked in a straight posture by mechanical constraint during S3. Constraint condition for the relative knee angle of the swing leg $\theta_{K2} = -(\theta_3 - \theta_4)$ is described as

$$-\left(\dot{\theta}_3 - \dot{\theta}_4\right) = 0. \tag{15}$$

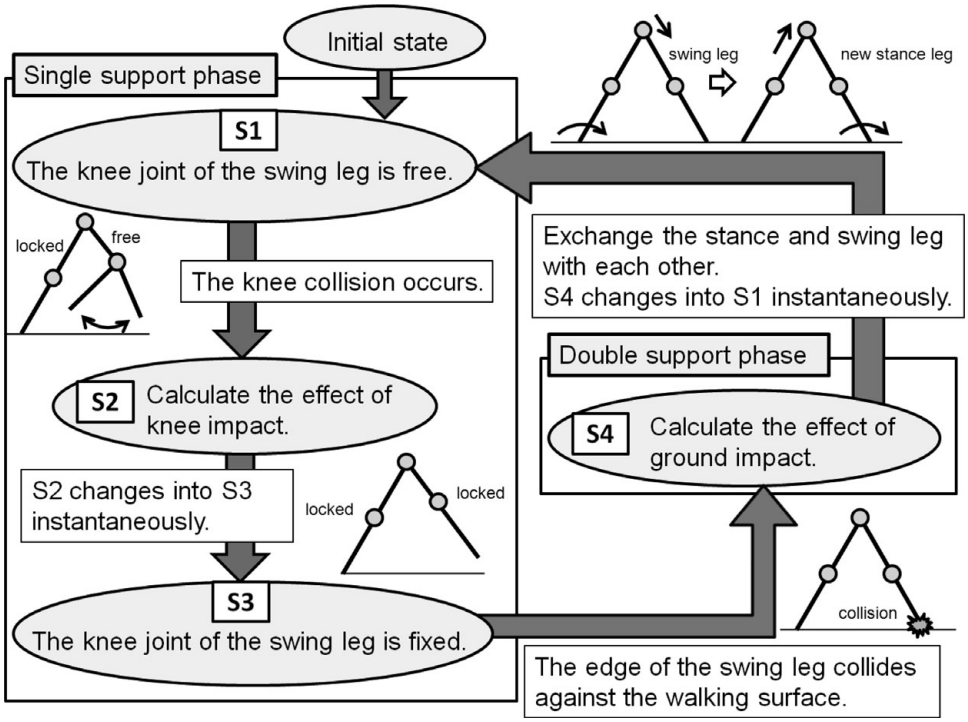


Fig. 7. The state transition diagram of dynamical walking. Dynamical walking of this robot has two phases. One is single support phase and another is double support phase. Single support phase consists of three states (S1–S3). Both S1 and S3 are continuous states in which the dynamical motion is calculated by numerical integration. S2 is discrete state jump that represents the instantaneous knee collision. Double support phase has one state (S4). S4 is discrete state jump that represents the instantaneous ground collision.

https://doi.org/10.1017/S0263574713000088 Published online by Cambridge University Press

Therefore, $\boldsymbol{J}_K(\boldsymbol{q})$ of S1 is

$$\boldsymbol{J}_K(\boldsymbol{q}) = \begin{bmatrix} 1 & 0 & 0 & -l_1\bar{C}_1 & -(l_2-R)\bar{C}_2 - R & 0 & 0 \\ 0 & 1 & 0 & l_1\bar{S}_1 & (l_2-R)\bar{S}_2 & 0 & 0 \\ 0 & 0 & 0 & 1 & -1 & 0 & 0 \end{bmatrix}, \tag{16}$$

and $\boldsymbol{J}_K(\boldsymbol{q})$ of S3 is

$$\boldsymbol{J}_K(\boldsymbol{q}) = \begin{bmatrix} 1 & 0 & 0 & -l_1\bar{C}_1 & -(l_2-R)\bar{C}_2 - R & 0 & 0 \\ 0 & 1 & 0 & l_1\bar{S}_1 & (l_2-R)\bar{S}_2 & 0 & 0 \\ 0 & 0 & 0 & 1 & -1 & 0 & 0 \\ 0 & 0 & 0 & 0 & 0 & 1 & -1 \end{bmatrix}, \tag{17}$$

where $\bar{C}_i = \cos\theta_i$ and $\bar{S}_i = \sin\theta_i$, $i = 1, 2$.

The instantaneous knee collision of S2 is described as

$$\boldsymbol{M}(\boldsymbol{q})\dot{\boldsymbol{q}}^+ = \boldsymbol{M}(\boldsymbol{q})\dot{\boldsymbol{q}}^- + \boldsymbol{J}_{CK}^{\mathrm{T}}(\boldsymbol{q})\boldsymbol{\lambda}_{CK},$$

where $\dot{\boldsymbol{q}}^-$ and $\dot{\boldsymbol{q}}^+$ denote velocities before and after the impact respectively. $\boldsymbol{\lambda}_{CK}$ denotes the constraint force to satisfy the constraint conditions after impact. $\boldsymbol{J}_{CK}(\boldsymbol{q})$ is equal to $\boldsymbol{J}_K(\boldsymbol{q})$ of Eq. (17). $\boldsymbol{\lambda}_{CK}$ is derived as

$$\boldsymbol{\lambda}_{CK} = -\left(\boldsymbol{J}_{CK}(\boldsymbol{q})\boldsymbol{M}(\boldsymbol{q})\boldsymbol{J}_{CK}^{\mathrm{T}}(\boldsymbol{q})\right)^{-1}\boldsymbol{J}_{CK}(\boldsymbol{q})\dot{\boldsymbol{q}}^-. \tag{18}$$

Therefore, $\dot{\boldsymbol{q}}^+$ is updated as

$$\dot{\boldsymbol{q}}^+ = -\left(\boldsymbol{I} - \boldsymbol{M}(\boldsymbol{q})\boldsymbol{J}_{CK}^{\mathrm{T}}(\boldsymbol{q}) \times \left(\boldsymbol{J}_{CK}(\boldsymbol{q})\boldsymbol{M}(\boldsymbol{q})\boldsymbol{J}_{CK}^{\mathrm{T}}(\boldsymbol{q})\right)^{-1}\boldsymbol{J}_{CK}\right)\dot{\boldsymbol{q}}^-. \tag{19}$$

Similarly, the instantaneous ground collision of S4 is described as

$$\boldsymbol{M}(\boldsymbol{q})\dot{\boldsymbol{q}}^+ = \boldsymbol{M}(\boldsymbol{q})\dot{\boldsymbol{q}}^- + \boldsymbol{J}_{CG}^{\mathrm{T}}\lambda_{CG},$$

where $\boldsymbol{\lambda}_{CG}$ denotes the constraint force to satisfy the constraint conditions after impact. $\boldsymbol{J}_{CG}$ is described as

$$\boldsymbol{J}_{CG}(\boldsymbol{q}) = \begin{bmatrix} 1 & 0 & 0 & 0 & 0 & -l_1\bar{C}_3 & -(l_4-R)\bar{C}_4 - R \\ 0 & 1 & 0 & 0 & 0 & l_1\bar{S}_3 & (l_4-R)\bar{S}_4 \\ 0 & 0 & 0 & 1 & -1 & 0 & 0 \\ 0 & 0 & 0 & 0 & 0 & 1 & -1 \end{bmatrix}, \tag{20}$$

where $\bar{C}_i = \cos\theta_i$ and $\bar{S}_i = \sin\theta_i$, $i = 3, 4$. Therefore, $\dot{\boldsymbol{q}}^+$ is updated as

$$\dot{\boldsymbol{q}}^+ = -\boldsymbol{N}\left(\boldsymbol{I} - \boldsymbol{M}(\boldsymbol{q})\boldsymbol{J}_{CG}^{\mathrm{T}}(\boldsymbol{q}) \times \left(\boldsymbol{J}_{CG}(\boldsymbol{q})\boldsymbol{M}(\boldsymbol{q})\boldsymbol{J}_{CG}^{\mathrm{T}}(\boldsymbol{q})\right)^{-1}\boldsymbol{J}_{CG}\right)\dot{\boldsymbol{q}}^-, \tag{21}$$

where $\boldsymbol{N}$ is the interchange matrix described as

$$\boldsymbol{N} = \begin{bmatrix} 1 & 0 & 0 & 0 & 0 & 0 & 0 \\ 0 & 1 & 0 & 0 & 0 & 0 & 0 \\ 0 & 0 & 1 & 0 & 0 & 0 & 0 \\ 0 & 0 & 0 & 0 & 0 & 1 & 0 \\ 0 & 0 & 0 & 0 & 0 & 0 & 1 \\ 0 & 0 & 0 & 1 & 0 & 0 & 0 \\ 0 & 0 & 0 & 0 & 1 & 0 & 0 \end{bmatrix}. \tag{22}$$

Similarly, new state vector $\boldsymbol{q}^+$ is updated as $\boldsymbol{q}^+ = \boldsymbol{N}\boldsymbol{q}^-$. $\boldsymbol{q}^-$ is the state vector before ground impact. In addition, new horizontal position of the hip joint x^+ is rewritten as

$$x^+ = l_1\sin\theta_1^+ + (l_2 - R)\sin\theta_2^+ + R\theta_2^+ \tag{23}$$

to update the origin of world coordinate. θ_1^+, θ_2^+ are elements of $\boldsymbol{q}^+$.

3.2. Control inputs

We treat the upper body and lower body of this robot as the upper pendulum and lower pendulum of the virtual inverted double pendulum respectively. We apply the parametric excitation of an inverted double pendulum to the robot. The concept of this virtual inverted double pendulum is shown in Fig. 8. From Fig. 8(a), the relationship between the lower body and the virtual lower pendulum is derived as

$$\begin{aligned} X_{GL} &= x - \tfrac{X_{GL1}}{M_g}, \\ Z_{GL} &= z - \tfrac{Z_{GL1}}{M_g}, \end{aligned} \tag{24}$$

where

$$M_g = m_H + m_1 + m_2 + m_3 + m_4, \tag{25}$$

$$\begin{aligned} X_{GL1} &= [(m_1a_1 + m_2l_1)\sin\theta_1 + m_2a_2\sin\theta_2 \\ &\quad + (m_3a_3 + m_4l_3)\sin\theta_3 + m_4a_4\sin\theta_4], \end{aligned} \tag{26}$$

$$\begin{aligned} Z_{GL1} &= [(m_1a_1 + m_2l_1)\cos\theta_1 + m_2a_2\cos\theta_2 \\ &\quad + (m_3a_3 + m_4l_3)\cos\theta_3 + m_4a_4\cos\theta_4], \end{aligned} \tag{27}$$

and

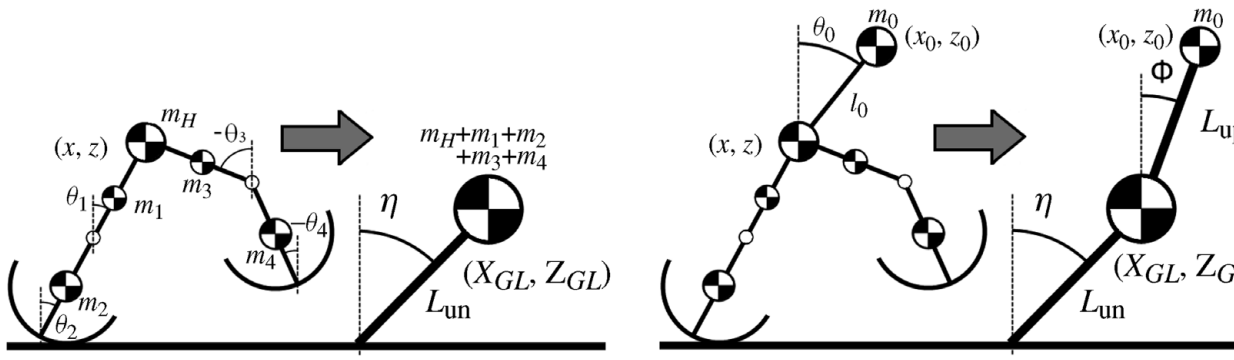
$$\begin{aligned} X_{GL} &= L_{UN}\sin\eta, \\ Z_{GL} &= L_{UN}\cos\eta, \end{aligned} \tag{28}$$

where $(X_{GL},\ Z_{GL})$ is the center of mass position of the lower body, and L_{UN} and η are the length and angle of the virtual lower pendulum respectively. Similarly, in Fig. 8(b), the relationship between the upper body and the virtual upper pendulum is derived as

$$\begin{aligned} x_0 &= x + l_0\sin\theta_0 = X_{GL} + L_{UP}\sin\phi, \\ z_0 &= z + l_0\cos\theta_0 = Z_{GL} + L_{UP}\cos\phi, \end{aligned} \tag{29}$$

$$l_0\sin(\theta_0 - \phi) = (Z - Z_{GL})\sin\phi - (X - X_{GL})\cos\phi, \tag{30}$$

https://doi.org/10.1017/S0263574713000088 Published online by Cambridge University Press



(a) The bipedal walking model and the virtual inverted pendulum. (b) The whole walking model and the virtual inverted double pendulum.

Fig. 8. The bipedal robot with an upper body and the virtual inverted double pendulum.

where $(x_0,\ z_0)$ is the mass position of the upper body, and L_{UP} and ϕ are the length and angle of the virtual upper pendulum respectively.

The motion of the lower body is controlled by parametric excitation control of an inverted pendulum.[9] The relative knee angle of the swing leg is controlled to move up and down the mass center of the lower body depending on the target pass. Desired function of the relative knee angle $\theta_{K2} = -\theta_3 + \theta_4$ is described as

$$\theta_{K2d}(\bar{x}) = \frac{\hat{A}}{1 + e^{-\alpha(\bar{x}-\beta_1)}} \times \frac{1}{1 + e^{\alpha(\bar{x}-\beta_2)}}, \tag{31}$$

$$\dot{\theta}_{K2d}(\bar{x}) = -\frac{\alpha \hat{A}\dot{\bar{x}}\left(e^{-\alpha(\bar{x}-\beta_1)} - e^{\alpha(\bar{x}-\beta_2)}\right)}{\left[1 + e^{\alpha(\beta_1-\beta_2)} + e^{-\alpha(\bar{x}-\beta_1)} + e^{\alpha(\bar{x}-\beta_2)}\right]^2}, \tag{32}$$

where $\bar{x}$ is the center of mass position of the lower body. From Eq. (29), the desired angle of the upper body θ_{0d} is derived as

$$\theta_{0d} = \phi_d + \sin^{-1}\left(\frac{(Z - Z_{GL})\sin\phi_d - (X - X_{GL})\cos\phi_d}{l_0}\right),$$

$$\dot{\theta}_{0d} = \frac{(\dot{Z} - \dot{Z}_{GL})\sin\phi_d - \left(\dot{X} - \dot{X}_{GL}\right)\cos\phi_d}{l_0\cos(\theta_0 - \phi_d)}, \tag{33}$$

where ϕ_d is the desired angle of the virtual upper pendulum. The purpose of this upper body control is to keep the angle of the virtual upper pendulum ϕ constant. Therefore, $\dot{\phi}_d = 0$ is assumed. Parametric excitation of an inverted double pendulum enables the robot to create the cooperative movement for the whole body through these control inputs. Numerical dynamical walking is simulated via these model and control inputs. Table II shows physical parameters of this robot.

Control input $\boldsymbol{u}$ and constraint force $\boldsymbol{\lambda}_K$ of S1 and S3 are derived as follows. From Eqs. (11), (16), and (17), following equations are obtained:

$$\ddot{\boldsymbol{q}} = \boldsymbol{M}^{-1}(\boldsymbol{q})\left[\boldsymbol{S}\boldsymbol{u} + \boldsymbol{J}_K^{\mathrm{T}}(\boldsymbol{q})\boldsymbol{\lambda}_K - \boldsymbol{h}(\boldsymbol{q}, \dot{\boldsymbol{q}})\right], \tag{34}$$

Table II. Physical parameters of the bipedal walker with an upper body.

Name	Value (unit)	Name	Value (unit)
m_H	8.00 (kg)	m_0	1.00–3.00 (kg)
m_1	1.00 (kg)	m_2	4.00 (kg)
m_3	1.00 (kg)	m_4	4.00 (kg)
R	0.40 (m)	l_0	0.50 (m)
l_1	0.50 (m)	l_2	0.50 (m)
l_3	0.50 (m)	l_4	0.50 (m)
a_1	0.25 (m)	a_2	0.25 (m)
a_3	0.25 (m)	a_4	0.25 (m)
A	−1.00 (rad)	α	70.0 (–)
β_1	−0.03 (m)	β_2	0.12 (m)

$$\begin{aligned}\boldsymbol{J}_K(\boldsymbol{q})\dot{\boldsymbol{q}} &= 0,\\ \boldsymbol{J}_K(\boldsymbol{q})\ddot{\boldsymbol{q}} &= -\dot{\boldsymbol{J}}_K(\boldsymbol{q})\dot{\boldsymbol{q}}.\end{aligned} \tag{35}$$

From Eqs. (34) and (35), constraint force $\boldsymbol{\lambda}_K$ is derived as

$$\begin{aligned}\boldsymbol{\lambda}_K &= -\boldsymbol{H}_1^{-1}(\boldsymbol{q})\left\{\dot{\boldsymbol{J}}_K(\boldsymbol{q})\dot{\boldsymbol{q}}\right.\\ &\quad \left.+\boldsymbol{J}_K(\boldsymbol{q})\boldsymbol{M}^{-1}(\boldsymbol{q})\left[\boldsymbol{S}\boldsymbol{u} - \boldsymbol{h}(\boldsymbol{q}, \dot{\boldsymbol{q}})\right]\right\},\\ \boldsymbol{H}_1(\boldsymbol{q}) &= \boldsymbol{J}_K(\boldsymbol{q})\boldsymbol{M}^{-1}(\boldsymbol{q})\boldsymbol{J}_K^{\mathrm{T}}(\boldsymbol{q}).\end{aligned} \tag{36}$$

In addition, we introduce the following two matrices, $\boldsymbol{H}_2(\boldsymbol{q})$ and $\boldsymbol{H}_3(\boldsymbol{q})$,

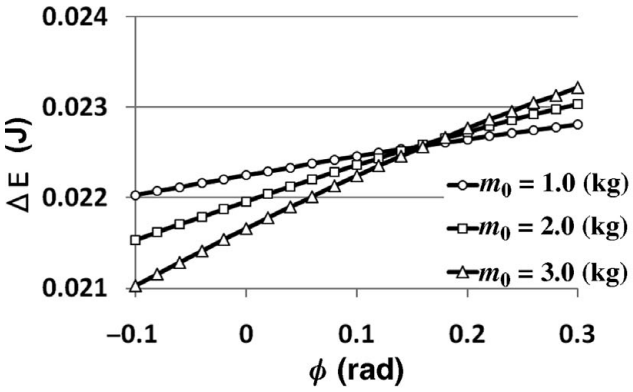
$$\boldsymbol{H}_2(\boldsymbol{q}) = \boldsymbol{M}_{(\boldsymbol{q})}^{-1}\left[\boldsymbol{I} - \boldsymbol{J}_K^{\mathrm{T}}(\boldsymbol{q})\boldsymbol{H}_1^{-1}(\boldsymbol{q})\boldsymbol{J}_K(\boldsymbol{q})\boldsymbol{M}_{(\boldsymbol{q})}^{-1}\right], \tag{37}$$

$$\boldsymbol{H}_3(\boldsymbol{q}, \dot{\boldsymbol{q}}) = \boldsymbol{M}^{-1}(\boldsymbol{q})\boldsymbol{J}_K^{\mathrm{T}}(\boldsymbol{q})\boldsymbol{H}_1^{-1}(\boldsymbol{q})\dot{\boldsymbol{J}}_K(\boldsymbol{q})\dot{\boldsymbol{q}}. \tag{38}$$

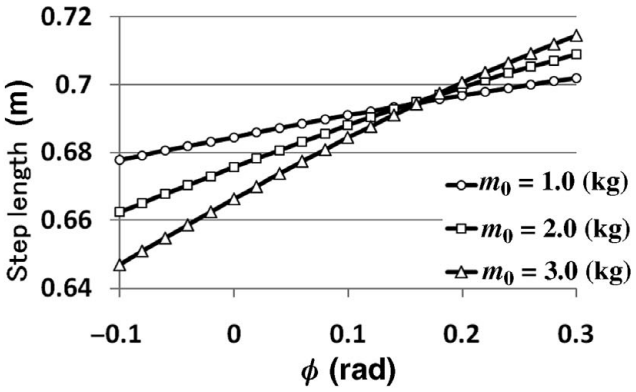
From Eqs. (34), (36), (37), and (38), control input $\boldsymbol{u}$ is derived as

$$\begin{aligned}\boldsymbol{u} &= \left(\boldsymbol{S}^{\mathrm{T}}\boldsymbol{H}_2(\boldsymbol{q})\boldsymbol{S}\right)^{-1}\left\{\boldsymbol{S}^{\mathrm{T}}\ddot{\boldsymbol{q}}_d\right.\\ &\quad \left.+\boldsymbol{S}^{\mathrm{T}}\left[\boldsymbol{H}_2(\boldsymbol{q})\boldsymbol{h}(\boldsymbol{q}, \dot{\boldsymbol{q}}) + \boldsymbol{H}_3(\boldsymbol{q}, \dot{\boldsymbol{q}})\right]\right\},\end{aligned} \tag{39}$$

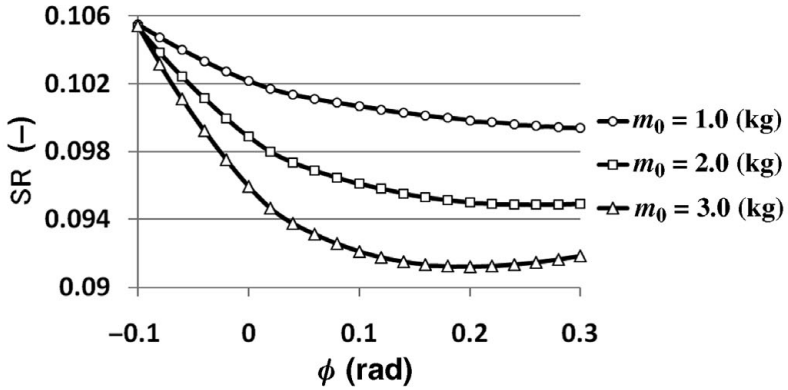
https://doi.org/10.1017/S0263574713000088 Published online by Cambridge University Press



(a) Increased mechanical energy.



(b) Walking step length.



(c) Specific resistance.

Fig. 9. Bipedal walking simulation results.

where $\boldsymbol{S}^{\mathrm{T}}\ddot{\boldsymbol{q}}_d$ of S1 is described as

$$\boldsymbol{S}^{\mathrm{T}}\ddot{\boldsymbol{q}}_d = \begin{bmatrix} k_{d1}\left(\dot{\theta}_{0d} - \dot{\theta}_0\right) + k_{p1}\left(\theta_{0d} - \theta_0\right) \\ k_{d2}\left(\dot{\theta}_{Kd} - \dot{\theta}_K\right) + k_{p2}\left(\theta_{Kd} - \theta_K\right) \end{bmatrix}, \quad \boldsymbol{S} = \begin{bmatrix} 0 & 0 & 1 & 0 & 0 & 0 & 0 \\ 0 & 0 & 0 & 0 & 0 & 1 & -1 \end{bmatrix}^{\mathrm{T}}, \tag{40}$$

and $\boldsymbol{S}^{\mathrm{T}}\ddot{\boldsymbol{q}}_d$ of S3 is described as

$$\boldsymbol{S}^{\mathrm{T}}\ddot{\boldsymbol{q}}_d = k_{d1}\left(\dot{\theta}_{0d} - \dot{\theta}_0\right) + k_{p1}\left(\theta_{0d} - \theta_0\right), \quad \boldsymbol{S} = [0 \quad 0 \quad 1 \quad 0 \quad 0 \quad 0 \quad 0]^{\mathrm{T}}. \tag{41}$$

4. Simulation Results

Simulation results are shown in Fig. 9. Fig. 9(a), (b), and (c) represent increased mechanical energy ΔE, walking step length, and specific resistance (SR) respectively. Specific resistance is the indicator of energy efficiency and is calculated as

$$\mathrm{SR} = \frac{\int_{0^+}^{T^-} (|\dot{\boldsymbol{q}}^{\mathrm{T}}\boldsymbol{S}^{\mathrm{T}}\boldsymbol{u}|)\mathrm{dt}}{M_g g \Delta X_g}, \tag{42}$$

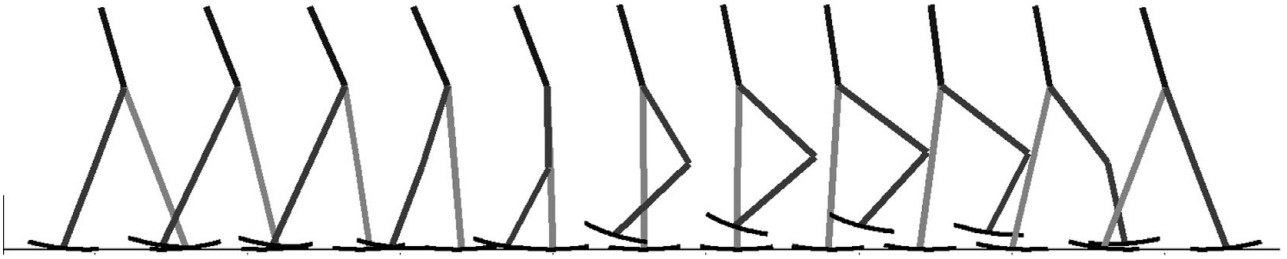
where T^- is the walking step time, M_g is the total mass of the target system, and ΔX_g is the horizontal moving distance of the mass center during one walking step. Numerator of Eq. (42) shows the actuator work, and SR shows the amount of energy that the system requires to move unit distance when the mass of the system is unit weight. Therefore, the locomotive system is efficient when SR is small. From Fig. 9, both ΔE and walking step length increased monotonically when the target angle of the virtual upper pendulum enlarged. The denominator of Eq. (42) increases when the step length enlarged. Therefore, SR decreased when the target angle of the virtual upper pendulum enlarged. However, SR became large when $\phi_d > 0.26$ (rad), $m_0 = 2.0$ (kg) and $\phi_d > 0.20$ (rad), $m_0 = 3.0$ (kg). The reason is that the robot required larger torque to maintain the upper body because the gravitational moment of the upper body enlarged. In addition, Table III shows simulation results of the robot without an upper body.

Table III. Specific resistance of robot without an upper body.

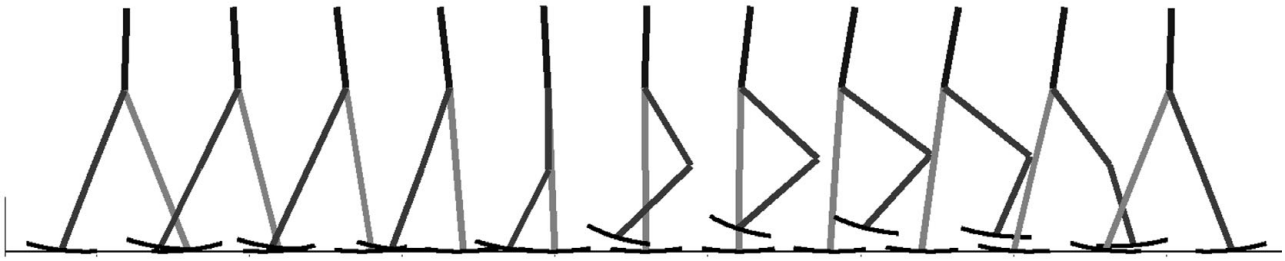
m_H	SR
8.0 + 1.0 (kg)	0.1026 (–)
8.0 + 2.0 (kg)	0.0997 (–)
8.0 + 3.0 (kg)	0.0972 (–)

In these cases, mass of the upper body was included in the mass of the hip joint. From Table III, when we set suitable target angle of the virtual upper pendulum, the robot with an upper body was able to walk more efficiently than the robot without an upper body. These results show that

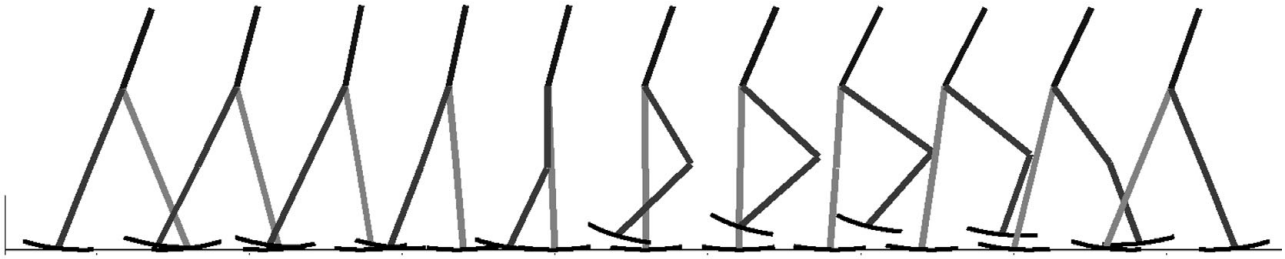
https://doi.org/10.1017/S0263574713000088 Published online by Cambridge University Press



(a) $\phi_d = -0.1$ (rad).



(b) $\phi_d = 0.0$ (rad).



(c) $\phi_d = 0.1$ (rad).

Fig. 10. Stick diagrams of walking behavior with respect to $m_0 = 3.0$ (kg) and the three values of ϕ_d.

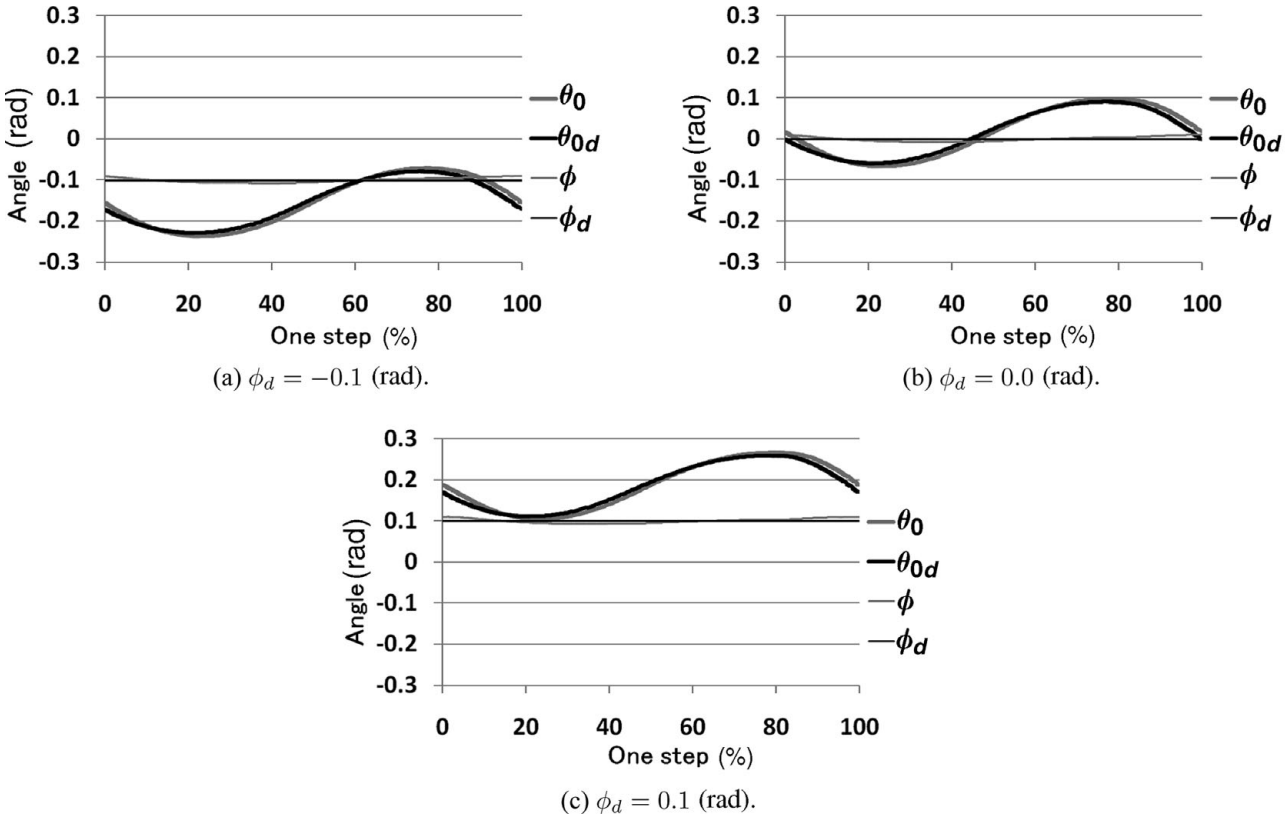
parametric excitation of an inverted double pendulum is valid for the bipedal walking. Therefore, proposed control strategy enables the bipedal robot to utilize its upper body to achieve energy efficient walking. Fig. 10 shows diagrams of the three walking behaviors during one step. From these diagrams, the upper bodies had similar behavior with each other. Fig. 11 shows the three simulated angles of the upper body and virtual upper pendulum angle with these target angles. It was found from Fig. 11 that the upper body behavior had the characteristics similar to sine curve although the virtual upper pendulum was maintained in constant posture. This feature of the upper body is also observed by human walking.[26] From Eq. (30), when the center of mass position of the lower body is lower than the hip joint position, the difference between the angle of the upper body θ_0 and the angle of the virtual upper pendulum ϕ enlarges. Therefore, the difference between θ_0 and ϕ is reduced when the center of mass position of the lower body approaches the hip joint. In this case, the effect of gravitational moment is reduced, which enables the robot to achieve more efficient walking.

In addition to these results, we observed that the value of SR is 0.0516 when the robot has the heavy upper body $m_0 = 15.0$ (kg) and the physical parameters ($m_1 = m_3 = 1.5$ (kg), $m_2 = m_4 = 3.5$ (kg), $a_1 = a_3 = 0.1$ (m), $a_2 = a_4 = 0.2$ (m), and $\phi_d = 0.2$ (rad)). Table IV shows several locomotive costs of bipedal robots.[23–25] From Table IV, most walkers have its locomotive cost from 0.05 to 0.14. Our method enables the bipedal walker with the upper body to achieve dynamic walking whose efficiency is close to human walking. In addition, the robot also achieves stable walking whose efficiency is similar to or greater than other bipedal walkers with the upper body. Therefore, we suggest that our method is valid for one of the efficient walking approaches.

Table IV. Comparison of locomotive cost.

Name	Locomotive cost
RABBIT	0.38
MABEL	0.14
Synthetic wheel biped	0.128
TU Delft Denise	0.08
MIT Spring Flamingo	0.07
Cornell Collins biped	0.055
Human	0.05

https://doi.org/10.1017/S0263574713000088 Published online by Cambridge University Press



(a) $\phi_d = -0.1$ (rad). (b) $\phi_d = 0.0$ (rad).

(c) $\phi_d = 0.1$ (rad).

Fig. 11. Target and simulated angles of upper body and virtual upper pendulum with respect to $m_0 = 3.0$ (kg) and three values of ϕ_d.

5. Conclusion

In this paper we proposed parametric excitation of an inverted double pendulum to consider the whole body behavior. Parametric excitation of an inverted double pendulum has the characteristic that maintaining the upper pendulum angle at a constant positive value contributes to parametric excitation. We analyzed the relationship between this characteristic and asymmetric property of parametrically excited inverted pendulum. Then we applied parametric excitation of an inverted double pendulum to the bipedal walker with an upper body. We verified the validity of proposed parametric excitation for bipedal walking via numerical simulation. As a result, the robot achieved more energy efficient walking when the desired upper pendulum angle enlarged. The robot with a heavy upper body achieved the dynamical stable walking whose efficiency is close to human walking. In addition, the robot also achieves the stable walking whose efficiency is similar to or greater than other bipedal walkers with the upper body. Consequently, we suggested that parametric excitation of an inverted double pendulum enables the bipedal robot to achieve energy efficient walking. In addition, we found that the upper body behavior had the characteristics similar to sine curve. We showed the improvement plan with respect to mass distribution to realize more energy efficient walking.

References

1. T. McGeer, "Passive dynamic walking," *Int. J. Robot. Res.* **57**(2), 62–82 (1990).
2. F. Asano, Z. W. Luo and S. Hyon, "Parametric Excitation Mechanisms for Dynamic Bipedal Walking," *Proceedings of the IEEE International Conference on Robotics and Automation* (2005).
3. F. Asano, T. Hayashi, Z. W. Luo, S. Hirano and A. Kato, "Parametric Excitation Approaches to Efficient Bipedal Walking," *Proceedings of the IEEE/RSJ International Conference on Intelligent Robots and Systems* (2007).
4. F. Asano and Z. W. Luo, "Energy-efficient and high-speed dynamic biped locomotion based on principle of parametric excitation," *IEEE Trans. Robot.* **24**(6), 1289–1301 (2008).
5. Y. Harata, F. Asano, K. Taji and Y. Uno, "Biped Gait Generation Based on Parametric Excitation by Knee-Joint Actuation," *Proceedings of the IEEE/RSJ International Conference on Intelligent Robots and Systems* (2007).
6. Y. Harata, F. Asano, K. Taji and Y. Uno, "Efficient Parametric Excitation Walking with Delayed Feedback Control," *Proceedings of the IEEE/RSJ International Conference on Intelligent Robots and Systems* (2009).
7. Y. Harata, F. Asano, Z. W. Luo, K. Taji and Y. Uno, "Biped gait generation based on parametric excitation by knee-joint actuation," *Robotica* **27**, 1063–1073 (2009).
8. T. Honjo, Z. W. Luo and A. Nagano, "Parametric Excitation of a Biped Robot as an Inverted Pendulum," *Proceedings of IEEE/RSJ 2008 International Conference on Intelligent Robots and Systems* (2008).
9. T. Honjo, T. Hayashi, A. Nagano and Z. W. Luo, "Target Trajectory Design of Parametrically Excited Inverted Pendulum for Efficient Bipedal Walking," *Proceedings of the International Conference on Control, Automation, Robotics and Vision* (2011).
10. M. Wisse, A. L. Schwab and F. C. T. van der Helm, "Passive dynamic walking model with upper body," *Robotica* **22**, 681–688 (2004).

https://doi.org/10.1017/S0263574713000088 Published online by Cambridge University Press

11. M. Wisse, D. G. E. Hobbelen and A. L. Schwab, "Adding an upper body to passive dynamic walking robots by means of a bisecting hip mechanism," *IEEE Trans. Robot.* **23**(1), 112–123 (2007).
12. T. Narukawa, M. Takahashi and K. Yoshida, "Numerical simulations of level-ground walking based on passive walk for planar biped robots with torso by hip actuators," *JSME J. Syst. Des. Dyn*. **2**(2), 463–474 (2008).
13. T. Narukawa, M. Takahashi and K. Yoshida, "Efficient walking with optimization for a planar biped walker with a torso by hip actuators and springs," *Robotica* **29**, 641–648 (2011).
14. E. K. Lavrovskii and A. M. Formalskii, "Optimal control of the pumping and damping of swing," *J. Appl. Math. Mech.* **57**(2), 311–320 (1993).
15. T. Hayashi, F. Asano, Z. W. Luo, A. Nagano, K. Kaneko and A. Kato, "Experimental Study of a Parametrically Excited Dynamical Bipedal Walker with Counterweights," *Proceedings of the IEEE/RSJ International Conference on Intelligent Robots and Systems* (2009).
16. T. Hayashi, K. Kaneko, F. Asano and Z. W. Luo, "Experimental Study of Dynamic Bipedal Walking Based on the Principle of Parametric Excitation with Counterweights," *Adv. Robot.* **25**, 273–287 (2011).
17. T. Hayashi, T. Honjo, A. Nagano and Z. W. Luo, "Asymmetric parametric excitation mechanism for biped robot," *J. Robot. Soc. Japan* **30**(2), 173–179 (2012) (in Japanese).
18. F. Asano, "Dynamic Gait Generation of Telescopic-Legged Rimless Wheel Based on Asymmetric Impact Posture," *Proceedings of the 9th IEEE-RAS International Conference on Humanoid Robots* (2009).
19. J. Rummel, Y. Blum, H. M. Maus, C. Rode and A. Seyfarth, "Stable and Robust Walking with Compliant Legs," *Proceedings of the IEEE International Conference on Robotics and Automation* (2010).
20. A. Merker, J. Rummel and A. Seyfarth, "Stable walking with asymmetric legs," *Bioinspiration & Biomimetics* **6**(4), 045004 (2011).
21. H. Dong, M. Zhao and N. Zhang, "High-speed and energy-efficient biped locomotion based on virtual slope walking," *Auton. Robots* **30**(2), 199–216 (2011).
22. T. Das and R. Mukherjee, "Dynamic analysis of rectilinear motion of a self-propelling disc with unbalance masses," *Trans. ASME J.* **68**(1), 58–66 (2001).
23. L. L. Flynn, R. Jafari and R. Mukherjee, "Active synthetic-wheel biped with torso," *IEEE Trans. Robot.* **26**(5), 816–826 (2010).
24. K. Sreenath, H. W. Park, I. Poulakakis and J. W. Grizzle, "A compliant hybrid zero dynamics controller for stable, efficient and fast bipedal walking on MABEL," *Int. J. Robot. Res.* **30**(9), 1170–1193 (2010).
25. S. Collins, A. Ruina, R. Tedrake and M. Wisse, "Efficient bipedal robots based on passive-dynamic walkers," *Science* **307**, 1082–1085 (2005).
26. J. P. Ferreira, M. M. Crisóstomo and A. P. Coimbra, "Human gait acquisition and characterization," *IEEE Trans. Instrum. Meas.* **58**(9), 2979–2988 (2009).

https://doi.org/10.1017/S0263574713000088 Published online by Cambridge University Press